EUROPEAN COMMISSION

Community research

BELBaR

(Contract Number: 295487)

DELIVERABLE (D-N°: D2.8)

Final report on erosion processes under flowing water conditions

Author(s):

E. Hansen, M. Hedström, Clay Technology AB

T. Schatz, B+ Tech Oy

R. Červinka, J. Gondolli, ÚJV Řež, a. s.

Reporting period: **01/03/12 – 29/02/16**

Date of issue of this report: **12/06/15**

Start date of project: **01/03/12** Duration: 48 Months

Project co-funded by the European Commission under the Seventh Euratom Framework Programme for Nuclear Research &Training Activities (2007-2011)		
Dissemination Level		
PU	Public	PU
RE	Restricted to a group specified by the partners of the BELBaR project	
CO	Confidential, only for partners of the BELBaR project	

EURATOM

DISTRIBUTION LIST

Name	Number of copies	Comments
Christophe Davies (EC) BELBaR participants		

BELBaR Deliverable D2.8

This report contains contributions from three different research laboratories and partners in the BELBaR project, Clay Technology AB, B+ Tech Oy, ÚJV Řež, a.s. Each contribution is presented as delivered and the authors from the different laboratories draw conclusions regarding their own work. However, readers of this report may notice both similarities and differences in the way the different groups have approached the problem of studying erosion processes in bentonite/montmorillonite under flowing water conditions. Related studies can also be found in Deliverables D2.7 and D2.11.

Results from Clay Technology AB

Materials and methods

Material

The erosion studies reported here have been performed using Wyoming-type (Wy) montmorillonite extracted from MX-80 bentonite (American Colloid Co.). The montmorillonite was purified and ion-exchanged with NaCl or $CaCl_2$ to the homo-ionic form according to the procedure described in (Karnland *et al*. 2006). The purified montmorillonite is referred to as Wy-Me, where Me is the counter ion. The chemical formula for an ideal sodium montmorillonite, interlayer water excluded, can be written as $[(Si_{8-\alpha}Al_{\alpha})(Al_{4-\beta}Mg_{\beta})O_{20}(OH)_4]^{(\alpha+\beta)-}Na^{+}_{\alpha+\beta}$, where by definition the tetrahedral charge is lower than the octahedral charge ($\alpha<\beta$) and the sum of tetrahedral and octahedral charges fulfil $0.4<\alpha+\beta<1.2$ (Karnland *et al.* 2006). Most experiments in this study have been conducted using Wy-Na. There are two major reasons for working with Wy-Na: First, Na-montmorillonite show essentially unlimited swelling below the critical coagulation concentration (CCC), i.e. it turns into a sol, which is the reason for studying the erosion process under dilute conditions in the first place. Second, Wy-Na has the highest CCC (~20 mM NaCl) of all the clays investigated in Deliverable D4.7. Thus erosion rates obtained using Wy-Na are pessimistic estimates, compared to the conceivable future conditions in a High-Level Waste (HLW) repository. Wy-Ca, on the other hand, is not sol-forming (Birgersson *et al.* 2009) so in this study, erosion experiments using Wy-Ca have not been performed. However, mixed Ca/Na-montmorillonite was found to form sol and erode in deionized (DI) water when the Na^+ content was >20% of the cation exchange capacity (CEC) (Birgersson *et al.* 2009, Hedström et al. 2011) in line with earlier findings (Shainberg and Kaiserman 1969). We have therefore in our study included a Wy-Ca/Na montmorillonite prepared from mixing equal amount of powdered Wy-Ca and Wy-Na montmorillonite. In this montmorillonite 50% of CEC is compensated by Ca^{2+} and 50% by Na^+ and we will in general refer to this clay as Wy-50/50.

Equipment

The artificial fractures, made of poly(methyl methacrylate), were square with an inside width of 21 cm. In the set of experiments reported here, two apertures, 120 μm and 240 μm have been used. The artificial fracture is equipped with an inlet and outlet, allowing us to flow various solutions through the cell (Figure 1). Similar equipment has been used by Schatz et al (2013), but there are some differences, e.g., in our fracture system the clay can only take up water from the slit whereas in the B+ Tech equipment the clay may also be in contact with water through filters on top and bottom of the clay puck.

The artificial fractures used for erosion measurements were equipped with an additional in- and outlet at the outlet side thereby allowing for flushing the outlet slit collecting eroded

material that may gather there. At the center of the fracture system there is room for a clay puck of diameter 35 mm and thickness ~10 mm.
The amount of eroded montmorillonite was measured using a portable turbidimeter TN-100 from Eutech Instruments. The light source in the turbidimeter is an infrared-emitting (850 nm) diode. The intensity of the scattered light is directly converted to nephelometric turbidity units (NTU) by the instrument. At low clay concentrations (<5 g/L), the turbidity response have been found to be linear. The mass of eroded clay particles can thus be calculated through the equation $m_{clay}=(N \cdot V)/114$ where m_{clay} is the mass of the eroded clay (g), *N* is the turbidity (NTU) and V is the volume of the suspension (L) (Birgersson *et al*. 2009).

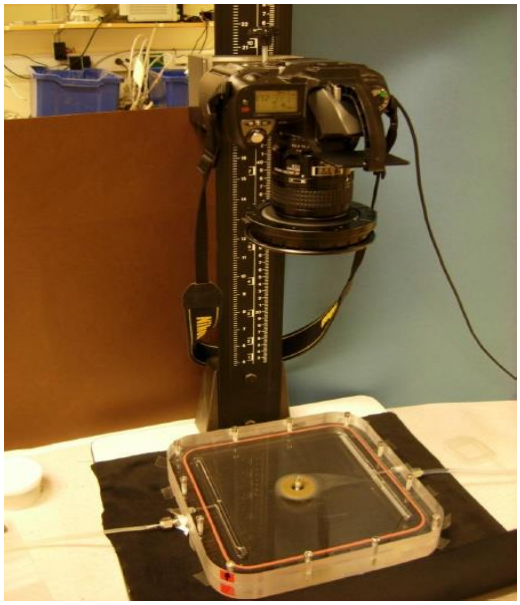

Figure 1. *Experimental set-up.*

Method
The montmorillonite was dried *in vacuo* overnight, followed by saturation with deionized water in a test cell similar to the ones used by ClayTech for measuring swelling pressures (Karnland *et al.* 2006). The initial dry density of the montmorillonite is 1257 kg/m^3 which gives a water-saturated density of 1800 kg/m^3. The water-saturated clay puck was transferred to the artificial fracture, with care taken not to allow the clay to dry. The fracture was closed and filled with degassed deionized water.
During free swelling experiments, the artificial fracture was filled with degassed DI water, after which the clay was allowed to swell into the fracture. This was photographically documented, with pictures taken at suitable intervals depending on the rate of expansion.
During erosion measurement experiments, aqueous solution, also prepared from degassed DI water, was flowed through the artificial fracture. The start- and end times of the erosion measurement were recorded. When the flow was stopped, the collected suspension was weighted. The outlet slit was flushed with degassed DI water to collect eroded material which had gathered in the outlet slit, and the flushed-through suspension was also weighted. Turbidity measurements were used to determine the amount of eroded colloidal clay particles in both water volumes.

Results and discussion

Free swelling – deionized water

The free swelling behavior was investigated at two different fracture apertures, 120 µm and 240 µm, in DI water. Initially, the swelling into the fracture progressed rapidly at both 120 µm and 240 µm. While the swelling progressively slows down, during the experimental time scale it does not cease completely. At 120 µm, closest to the clay puck we find a repulsive paste, quite well-defined and thick enough to appear very bright in color (scattered light from the camera flashes) (Figure 2a). This paste is strong enough that as it expands, it pushes air bubbles in the fracture ahead of itself, rather than surrounding them. Further out, there is a sol of varying (and not yet determined) clay concentration. At the interface between the sol and the DI water a fingering instability occur, akin to the Rayleigh-Taylor instability (RTI) that occurs when a denser liquid is placed on top of a less dense liquid and is pulled down by gravity. The RTI fingers are particularly well resolved in the thinner fracture Figure 2a. In this case it is not gravity that is the driving force for the RTI but water transport into the clay.

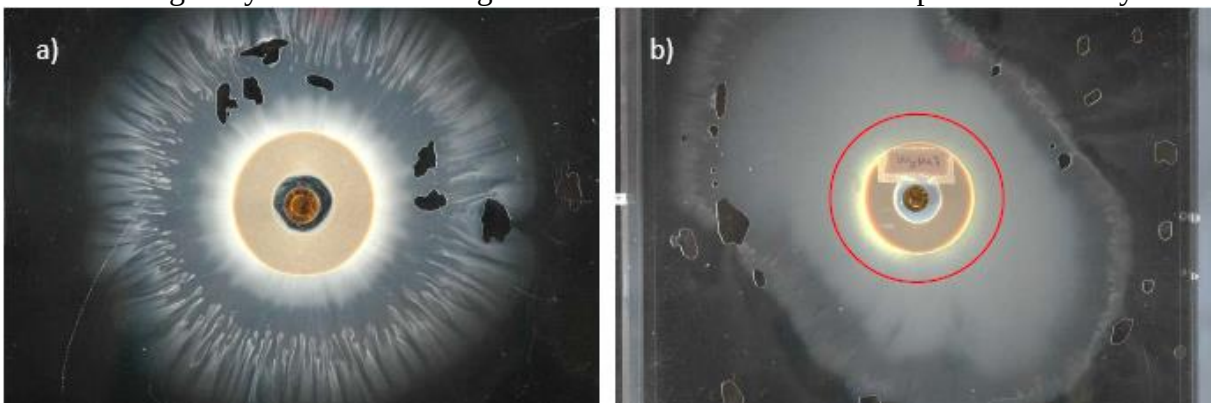

Figure 2. *Free swelling in deionized water after 30 days at a) 120 µm aperture and b) 240 µm aperture. The red circle in b) shows the extent of extrusion (swelling) of paste (the brighter area outside the montmorillonite puck in a) into the fracture at 120 µm for comparison. When there is a flow through the cell, all clay outside the brighter paste, is transported away.*

The same phases, the thick paste and the sol, are found during free swelling at an aperture of 240 µm (Figure 2b). Also RTI can be found, although the fingers are less well-resolved at the broader aperture. As in the case of 120 µm aperture, the paste is sufficiently thick to push air bubbles ahead during swelling rather than encompassing them. For comparison, the edge of the corresponding paste is outlined in Figure 2b, which gives an idea of the difference in swelling capability at different apertures.

The paste, i.e., the thicker clay phase closest to the puck, is found to withstand the shear forces and not erode under our conditions, even at the highest flow rates. However, as swelling is a continuous process, particles that disperse from the paste to form a sol are easily flowed away into the fracture.

Free swelling – 25 mM NaCl-solution

The free swelling behavior in a solution with higher salinity was also investigated. When setting up this experiment, clay was mechanically extruded into the fracture when the fracture was closed, thus the clay in the fracture has the same density as in the puck. This point constitutes the starting point for swelling, and has been outlined with a red circle in Figure 3. During the initial 48 h, some swelling (1-2 mm) is evident. Despite this, after the initial two days no more swelling is experienced and the clay appears to have formed a stable gel at the edges, which does not release sol particles into the fracture. Even with a flow of 25 mM

NaCl-solution, there are no signs of erosion. In fact, decreasing the salinity to 20, 15 or 10 mM NaCl still causes no erosion during flow. In order to see any sign of erosion, the salinity of the solution had to be decreased to 5 mM NaCl. This suggests the presence of some sort of hysteresis, which might affect the montmorillonite loss in the actual HLW repository.

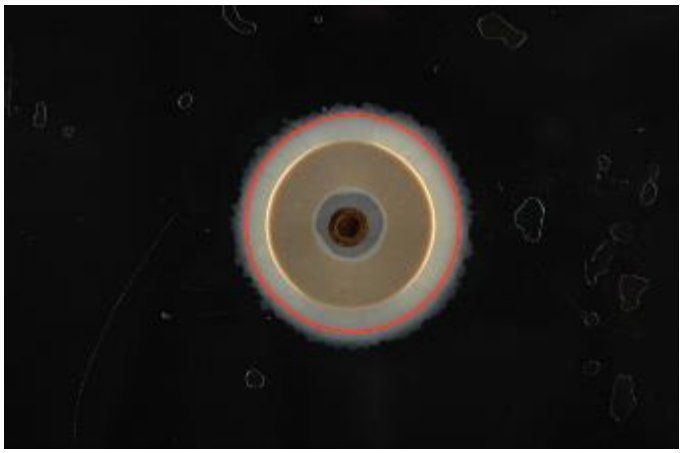

Figure 3. *Free swelling in 25 mM NaCl-solution at an aperture of 120 µm. The saturated density of the montmorillonite is 1800 kg/m^3*

Erosion measurement Wy-Na

Initial erosion measurements were performed at a fracture aperture of 120 µm (Figure 4). The measurements commenced at 5 mM NaCl (aq). As expected, since CCC is ~20 mM, the erosion was found to increase with increasing flow rate. By raising the salinity to 10 mM NaCl (aq), the erosion was decreased. However, it was still increasing with flow rate. After increasing the salinity to 15 mM NaCl (aq), the erosion during the first 48 h was roughly half the erosion at the corresponding flow rates at 10 mM NaCl.

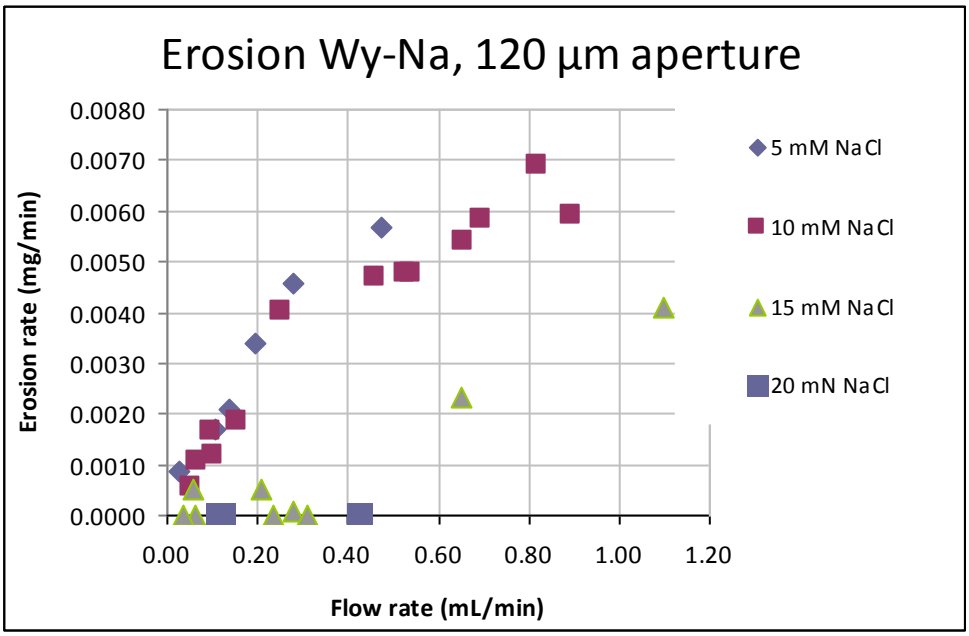

Figure 4. *Erosion of Wy-Na in an artificial fracture with aperture 120 µm. Salinity was increased from 5 mM NaCl to 20 mM NaCl.*

Within a week, erosion had completely ceased or was below the detection limit. The salinity was further increased to 20 mM NaCl, as 20 mM NaCl has been reported as the CCC value of Wyoming montmorillonite clay (Birgersson *et al*. 2009). As expected, there were no signs of erosion.

After the salinity had been increased from 5 mM NaCl to 20 mM NaCl, we decided to test if erosion would commence at 10 mM NaCl as previously erosion ceased upon increasing the salinity from 10 mM NaCl to 15 mM NaCl. The salinity of the aqueous solution was first decreased to 15 mM NaCl before erosion measurements at 10 mM NaCl was started. Despite the fact that the erosion measurements were performed during a month's time, which should have been ample time for the clay to reach a new Donnan equilibrium with the new solution (Birgersson and Karnland 2009; Karnland and Hedström, 2012), there were no signs of erosion during any of the measurements. Therefore, the salinity was decreased to 5 mM NaCl. Yet again, there were no signs of erosion during the initial measurements. However, after 16 days, erosion commenced. The erosion measurements were continued during two months, in order to investigate whether erosion during this time period reaches the erosion at the initial 5 mM NaCl-measurements. Despite this, the erosion did not appear to approach the earlier erosion levels (Figure 5). It is of course possible that given enough time, the erosion will be similar whether the NaCl-concentration is increased from deionized water, or decreased from a higher NaCl-concentration, but it is not obvious on this time scale. Consequently, there appear to be a considerable hysteresis effect, where the history of the clay sample appears to play a significant role in the erosion of montmorillonite clay. This illuminates the difficulty in reaching conclusions as to the CCC, the phase behavior or the erosion susceptibility of montmorillonite.

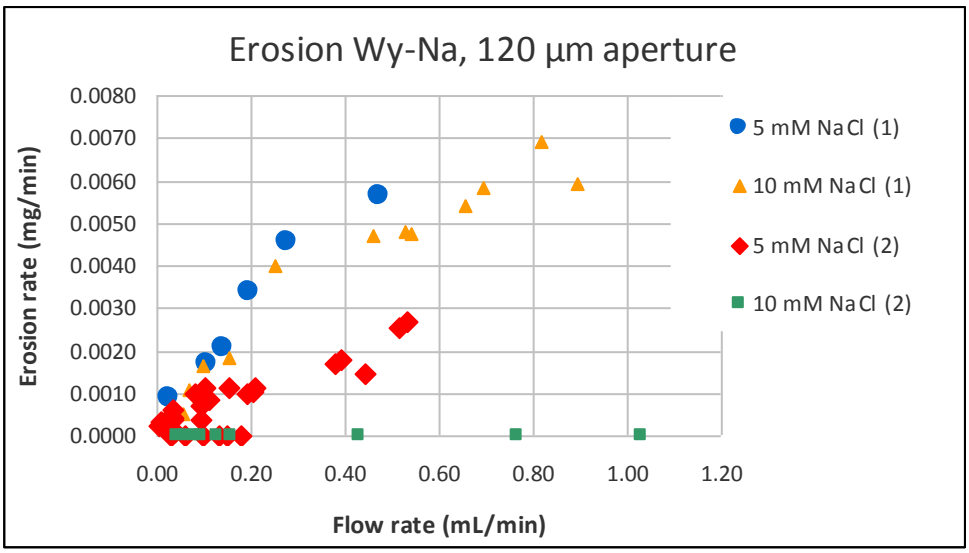

Figure 5. *Erosion rates v.s flow rate for the case where first the NaCl concentration in the flowing solution was increasing (1). After reaching 20 mM NaCl the concentration in the flowing solution was decreased (2).*

Erosion measurements at an aperture of 240 µm commenced with deionized water. When shifting to 5 mM NaCl-solution, the erosion difference at low flows was marginal, although the difference in erosion at higher flows was more significant (Figure 6).

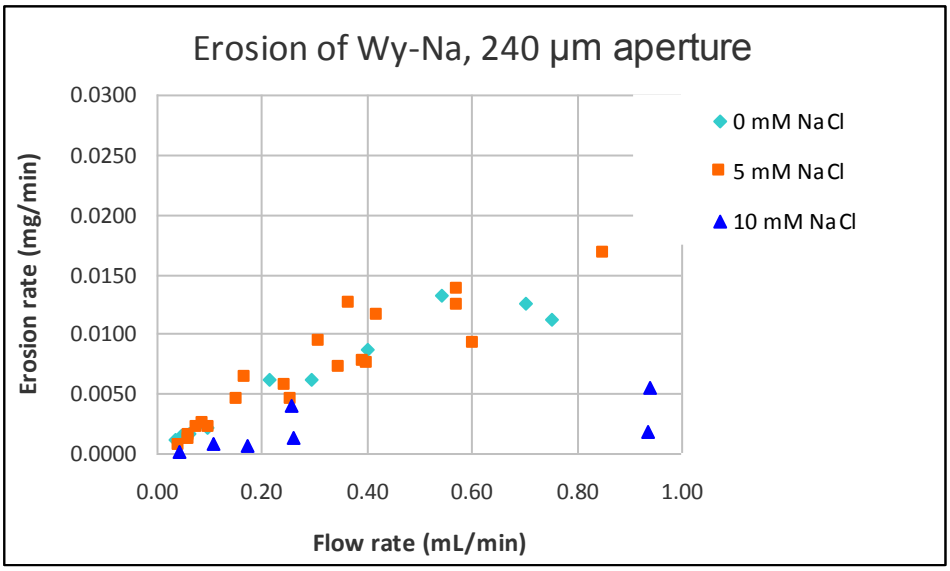

Figure 6. *Erosion of Wy-Na in an artificial fracture with aperture 240 µm. Salinity was increased from 0 mM NaCl to 10 mM NaCl.*

Comparison of erosion at different fracture apertures

When we compare the erosion at different fracture apertures, we find that the erosion depends on the fracture aperture as well as salinity. One has to take into account that in Figure 7 the erosion rate is plotted against flow rate given as volume per time, thus at the same flow rate the flow velocity at the larger aperture is lower. Without any clay present the velocity would be precisely a factor two lower in the 240 µm fracture compared to the 120 µm fracture at the same flow rate. Due to larger extrusion of clay in the wider fracture the ratio in flow rate must be less than a factor two. The results in Figure 7 show that at 5 mM, erosion rate is larger in the wider fracture also taking velocity into account. However at 10 mM NaCl the erosion rates vs. flow velocity are more or less the same for the two apertures.

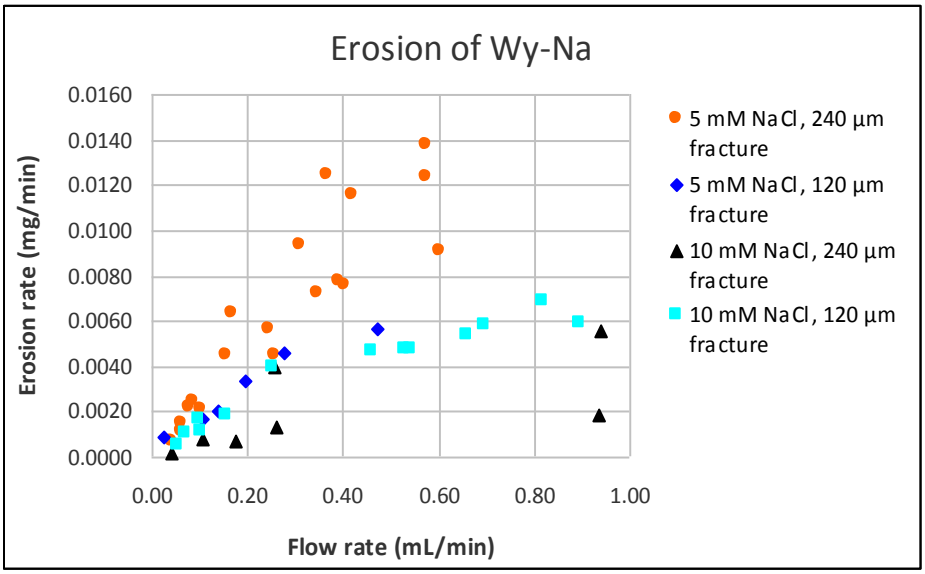

Figure 7. *Comparison of erosion rates of Wy-Na in artificial fractures with apertures 120 µm and 240 µm. Salinity was increased from 0 mM NaCl to 10 mM NaCl.*

Erosion from Wy-Ca/Na (Wy-50/50)-horizontal fracture

The mixed Wy-Ca/Na was water saturated in a test cell over a period of 9 days after which the montmorillonite puck was transferred to the artificial fracture setup (aperture 120µm). The montmorillonite was contacted to DI and degassed water and was left to swell for 36 days under stagnant water conditions. The general free swelling behavior of Wy-50/50 is similar to Wy-Na (Figure 2), with the development of RTI fingers at interface to the water. After the free-swelling period DI water was flushed through the fracture to remove the sol. Then measurements of erosion under flowing conditions started using saline water with ionic strength from 1 mM to 20 mM. The ionic strength was set by NaCl but in order to avoid ion-exchange a small amount of $CaCl_2$ was added (1µM to 10 µM depending on the NaCl concentration).

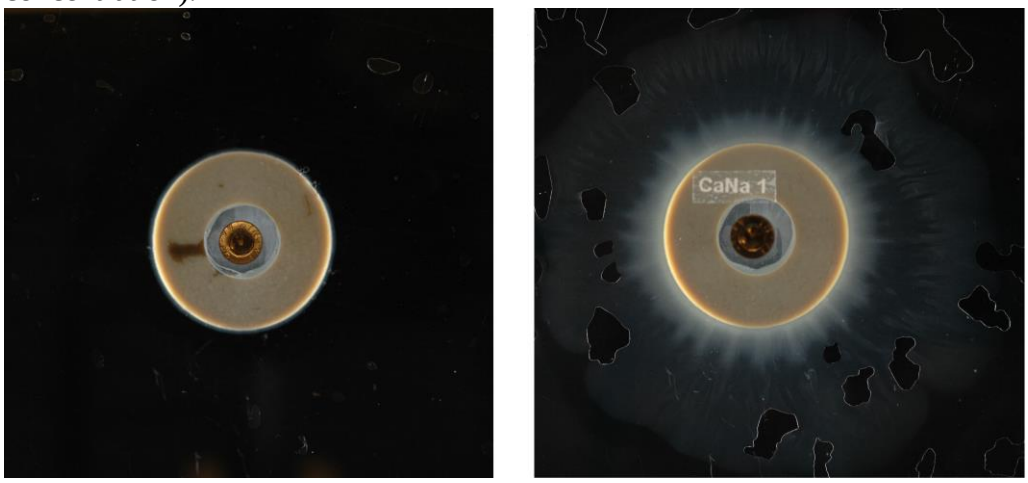

Figure 8. *Free swelling of Wy-50/50 in deionized water and aperture of 120 µm. Left: Initial state. Right: The state after 36 days. The gas bubbles visible in the right picture presumably originate from gas that was trapped around (above and under) the montmorillonite puck at installation.*

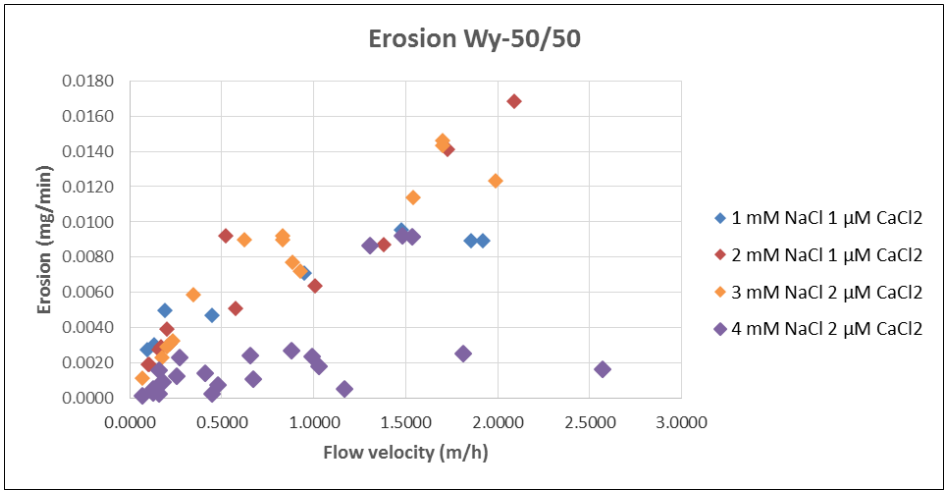

Figure 9. *Erosion of Wy-Ca/Na in an artificial fracture with aperture 120 µm. Salinity was increased from 1 mM NaCl to 4 mM NaCl. A small µM $CaCl_2$ concentration is included to prevent ion exchange during the tests.*

The results for ionic strength up to 4 mM are presented in Figure 9. For ionic strengths up to 3 mM the erosion rates behave similarly with erosion increasing with flow velocity and no noticeable dependence on salinity. At 4 mM the erosion in generally lower at all flow

velocities. Furthermore, there is no trend between flow velocity and erosion rate. There are three outliers in the 4 mM results (flow velocity ~1.5 m/h and erosion rates ~0.009 mg/min). Those measurements were made in the beginning after switching from 3 mM to 4 mM solution and most likely reflects the behavior of Wy-Ca/Na at 3 mM and are not representative for the equilibrium conditions at 4 mM. In general, the erosion rates at 4 mM scatter around 0.001 mg/min which are close to the lowest measured rates for Wy-Na at 5 and 10 mM NaCl (Figure 4), but in contrast to the results for Wy-Na the dependence on flow velocity is absent.

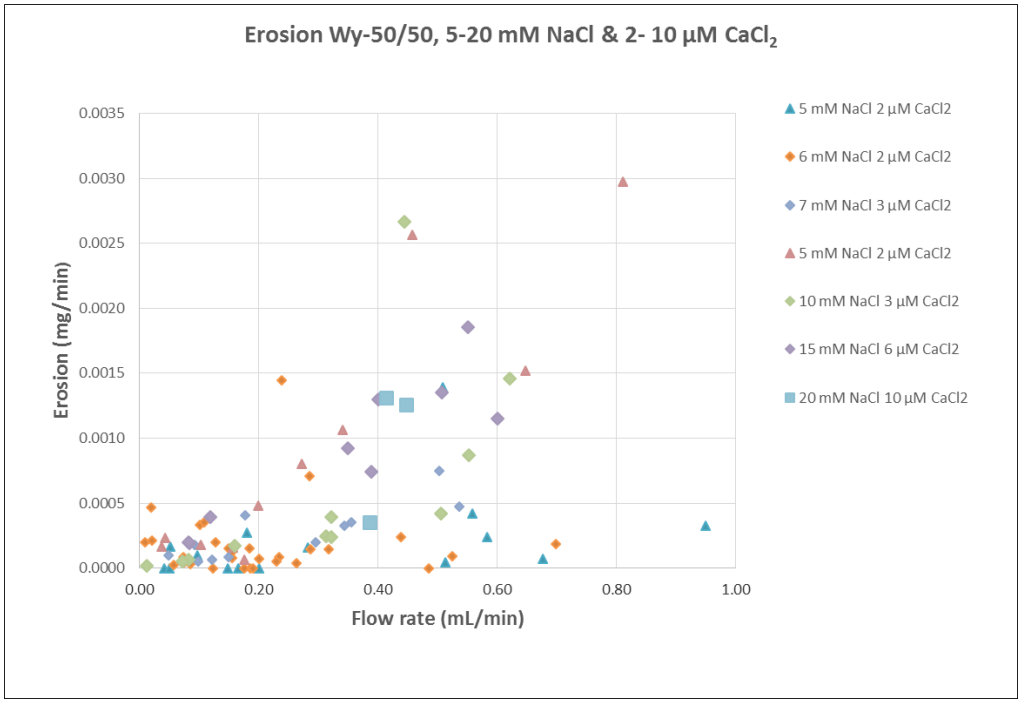

Figure 10. *Erosion of Wy-Ca/Na in an artificial fracture with aperture 120 µm. Salinity was changed according to the order in the legend. The lowest salinity was 5 mM and the highest 20 mM. A small µM $CaCl_2$ concentration is included to prevent ion exchange during the tests.*

The erosion did not stop at 4 mM so further tests at higher ionic strengths were conducted. Most measured erosion rates at ionic strengths between 5 and 20 mM were about a factor of two lower than the rates at 4 mM, but not showing any clear trend with increasing ionic strength (Figure 10). Possibly, there is a tendency that erosion increases for ionic strengths beyond 7 mM. After reaching 7 mM the ionic strength was lowered to 5 mM. The erosion rates measured at 5 mM after this change were higher than the erosion rates measured after ionic strength was increased from 4 to 5 mM. After the second period of erosion measurements at 5 mM the ionic strength was increased to 10, 15 and finally 20 mM. Interestingly, erosion did not stop even at 20 mM NaCl and 10 µM CaCl2.

At the lowest flow rates <0.2 mL/min all the erosion measurements in Figure 10 gave erosion rates below 0.0005 mg/min. With a diameter of the clay paste (initial puck + extruded zone) of 6 cm the above erosion rates correspond to a unit erosion rate of $3.7 \cdot 10^{-7}$ kg/m^2·s. Under the assumption of a fracture aperture in the repository of 1 mm and a diameter of the clay paste of 2 m, the above unit erosion rate corresponds to an erosive mass loss < 0.08 kg/yr.

Wy-Ca/Na in contact with Grimsel water simulant in horizontal and sloped fractures
We let Grimsel water (0.7 mM NaCl and 0.14 mM $CaCl_2$ in this study) represent glacial/post glacial conditions.

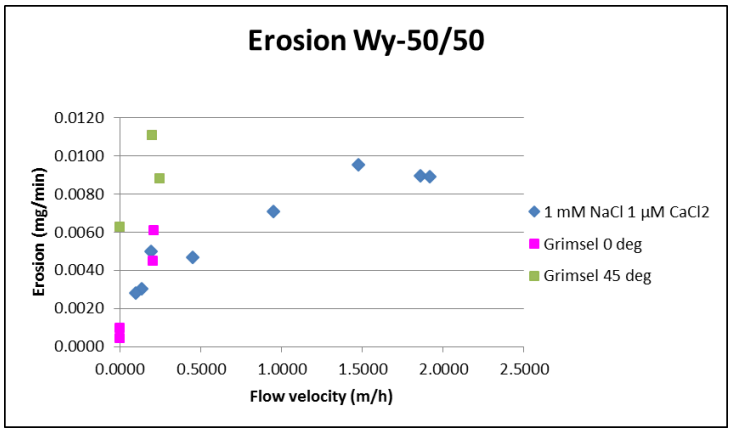

Figure 11 *Erosion of Wy-Ca/Na in an artificial fracture with aperture 120 µm. Grimsel water has ionic strength of 1.12 mM which is comparable to 1 mM NaCl.*

Figure 11 shows the results from erosion tests using Grimsel water together with the results from 1 mM NaCl. The erosion rates using Grimsel water and a horizontal fracture are comparable to the previous findings for 1 mM NaCl. The results at zero flow velocity were obtained in stagnant water over a period of several days. The eroded amount represent the sol surrounding the paste, and this material was collected by flushing the fracture for 15-30 minutes using high flow. The erosion rate at zero velocity was calculated by dividing the eroded mass with the time of free "expansion" (rather paste to sol transition). The total amount was ~8 mg both after 6 days of swelling and after 12 days. This suggests that the paste-to sol transition only progresses as long as the sol is removed. In stagnant water the sol is only diluted which is a diffusive process and therefore slow.
For a sloped fracture, the sol is constantly removed due to gravity. Note that the sol is a liquid phase of higher density than water and gravity acts on this liquid. This gives an erosion rate of an order of magnitude higher than the one measured after 12 days under stagnant conditions in a horizontal fracture. Using the example above of a clay paste with diameter of 2 m and a fracture aperture of 1 mm, the erosion from a sloped fracture (slope angle 45 degrees) amounts to approximately 1 kg/yr under glacial water conditions. Similar erosion rates was found in the experiments on sloped fractures performed at B +Tech (T. Schatz, Deliverable D2.5).

Conclusions

For Wy-Na we have confirmed the connection between the flow rate and the erosion, when the NaCl concentration is well below the CCC. As the salinity increases, erosion decreases. At an aperture of 120 µm, the erosion eventually ceases when the salinity in the system is 15 mM NaCl. For the aperture of 240 µm the test has not yet been performed above 10 mM but the tests at 10 mM NaCl indicate a clear reduction in erosion rate. In fact the erosion rates vs. flow velocity are the same for 120 and 240 µm apertures at 10 mM NaCl, possibly indicating the formation of stable structures at that salinity. However, more data are needed to verify this and to rule out other explanations.
Furthermore for Wy-Na, we see a hysteresis effect present, that is, the history of the clay will affect the erosion capability of the clay. That means that a montmorillonite clay that erodes at a salinity of 10 mM NaCl, might be completely stable against erosion, if it has previously had a higher salinity present, during which the clay particles at the clay-solution interface could form a gel. This suggests that not only is control of the boundary conditions of importance for evaluating erosion rates; awareness of the system's history seems also crucial. Erosion in sloped fractures showed an order of magnitude larger erosion rates compared to those obtained using horizontal fractures. As long as the sol is removed from the paste-sol interface,

erosion was found to progress under glacial water conditions. The erosion rate obtained using Wy-50/50 montmorillonite was found to be approximately 1 kg/yr when scaled up to repository conditions.

References

Birgersson M., Börgesson L., Hedström M., Karnland O., Nilsson U. (2009). Bentonite erosion – Final report. SKB Technical Report, TR-09-34, SKB Stockholm.

Birgersson M., Karnland O. (2009). Ion equilibrium between montmorillonite interlayer space and external solution –consequences for diffusional transport. Geochim. Cosmochim. Acta 73, 1908-1923.

Hedström M., Birgersson M., Nilsson U., Karnland O. (2011) Role of cation mixing in the sol formation of Ca/Na-montmorillonite. Phys. Chem. Earth 36, 1564-1571.

Hedström M., Karnland O. (2012). Donnan equilibrium in Na-montmorillonite from a molecular dynamics perspective. Geochim. Cosmochim. Acta 77, 266-274.

Karnland O., Olsson S., Nilsson U. (2006). Mineralogy and Sealing Properties of Various Bentonites and Smectite-rich Clay Material. SKB Technical Report, TR-06-30, SKB Stockholm.

Schatz T, Kanerva N, Martikainen J, Sane P, Olin M, Seppälä A, Koskinen K, (2013). Buffer erosion in dilute groundwater. POSIVA 2012-44. Posiva Oy, Olkiluoto, Finland.

Shainberg, I., Kaiserman, A. (1969). Kinetics of the formation and breakdown of Ca-montmorillonite tactoids. Soil Sci. Soc. Am. Proc. 33, 547–551.

Results from B+ Tech Oy.

Background

This report summarizes work conducted at B+Tech during the period from 1.6.2014 to 1.6.2015 of the BELBaR Project. The work described below is related to BELBaR deliverable D2.8 "Final report on erosion processes under flowing water conditions." Other, related work from B+Tech performed during this period is reported in BELBaR deliverables D2.7 "" and D2.11 "."

The work at B+Tech is conducted mainly using small-scale (24 cm × 24 cm fracture plane, 2 cm diameter × 2 cm height sample chamber), flow-through, artificial fracture systems in which swelling clay material can extrude/erode into a well-defined, intersecting fracture (see Figure 1). These experiments are performed in order to simulate the potential extrusion/erosion behavior of bentonite buffer material at a transmissive fracture interface. Using such systems the effect of solution chemistry (salt concentration and composition), material composition (sodium montmorillonite and admixtures with calcium montmorillonite, natural bentonites), flow velocity, fracture geometry (aperture, slope angle) and the role of accessory minerals on erosion processes can be analyzed.

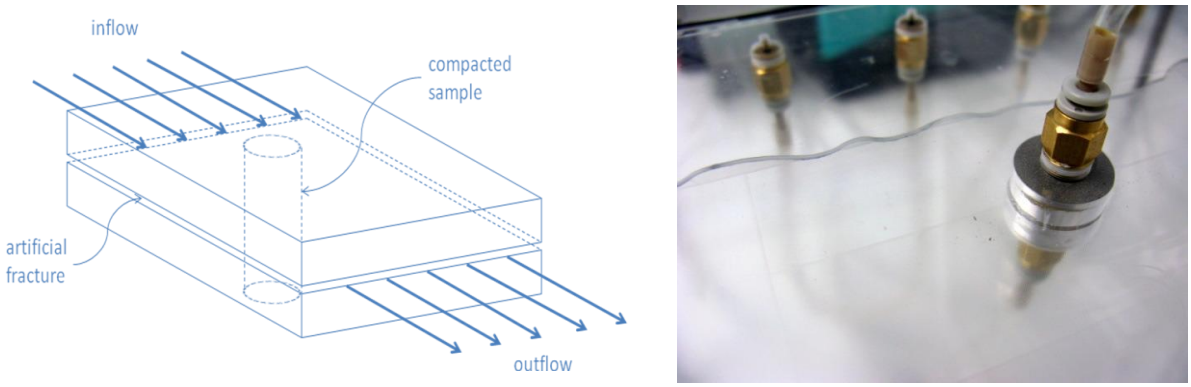

Figure 1. *Schematic representation of the flow-through, artificial fracture test system design basis (left) and photographic image of a flow front approaching a compacted sampled through a 1 mm aperture fracture (right).*

More recently the use of a larger artificial fracture cell was also started at B+Tech. This system is comprised of a roughly 1 m × 1 m fracture plane and a 5 cm diameter × 5 cm height sample chamber and allows for variable fracture aperture configuration.
Two similar tests have been conducted in both the large and small artificial fracture test systems positioned horizontally. Additionally, two (even more) similar tests have been conducted in both the large and small artificial fracture test systems positioned at a 45° slope angle (these results are compared in BELBaR deliverable D2.7). Specifically, the horizontal tests were run using washed MX-80 against a Grimsel groundwater simulant flowing through the fractures at ~0.09 ml/min. The aperture in the large fracture system was initially set to 0.1 mm and the aperture in the small system was configured to 1 mm. The same sample material was used in both cases, namely MX-80 bentonite washed free of soluble material and thoroughly exchanged with sodium cations, at the same compacted, dry density (~1.6 g/cm^3). The small fracture test was run for 865 hours and the large fracture test for 5304 hours (see Figure 2).

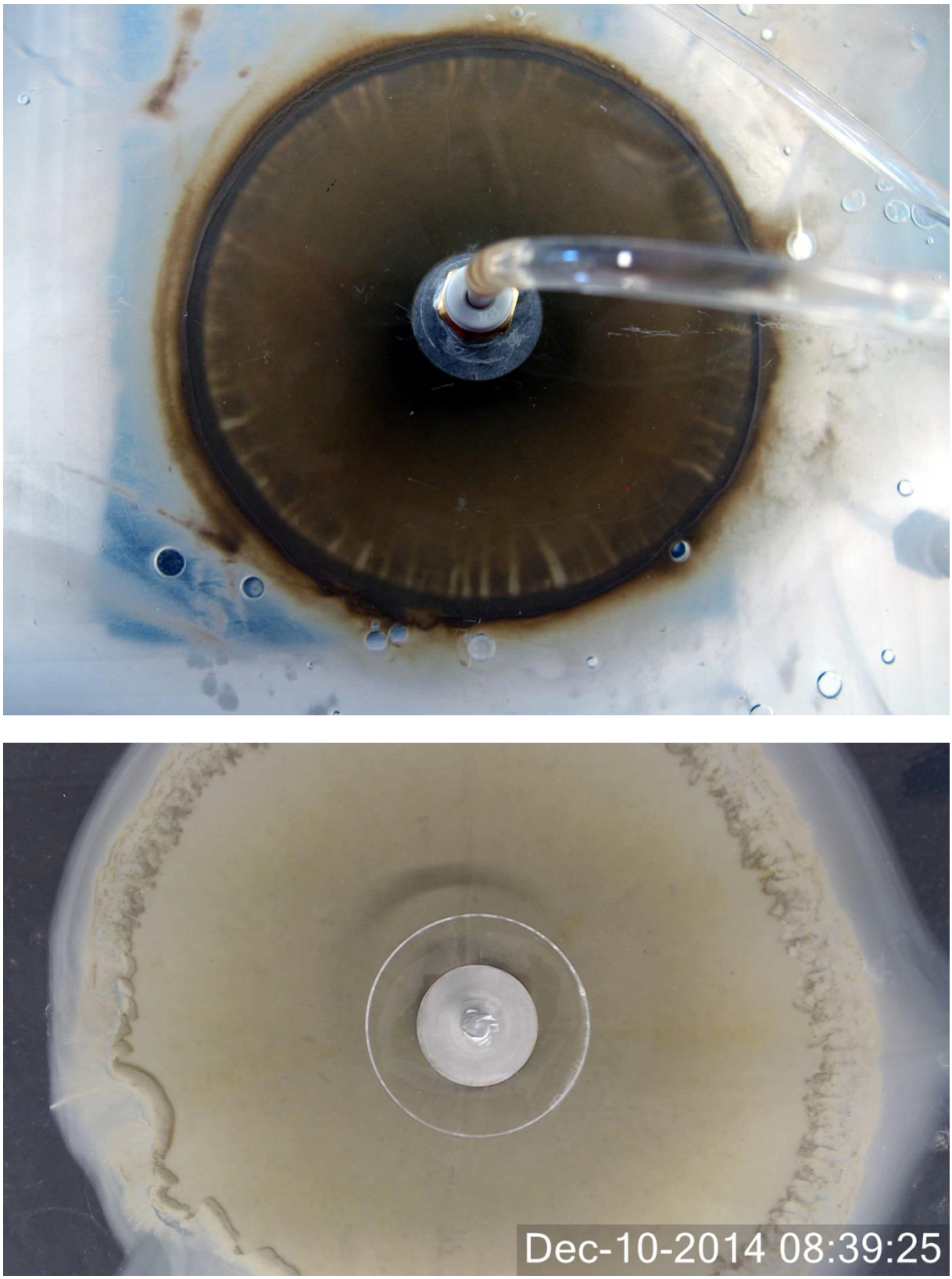

Figure 2. *Washed MX-80 bentonite in contact with a Grimsel groundwater simulant at an average flow rate of ~0.09 ml/min through the small fracture system with 1 mm aperture (upper image, taken at 865 h) and through the large fracture system with 0.1 mm aperture (lower image, taken at 5304 h).Note that the porous frits in the center of the images for scale; in the upper image the frit diameter is 2 cm and in the lower image it is 5 cm.*

Similar extrusion behaviour was observed in both systems in that sample material extruded rather uniformly out into the fractures and the extrusion distances increased over time (see Figure 3). In the case of the small fracture system, a steady-state extrusion diameter of ~10 cm was reached after approximately 185 hours. No such limiting value was observed in the large fracture system even after 5304 hours.

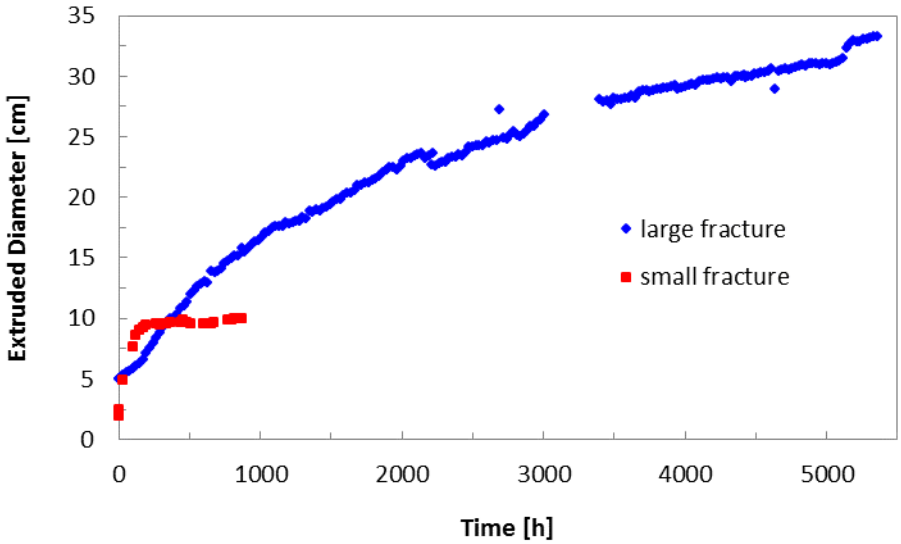

Figure 3. *Extrusion (diameter) observed over the course of the large and small fracture system tests with washed MX-80 bentonite against Grimsel groundwater simulant.*

The effluent solids content collected from the fracture outflows over the course of the large and small fracture system tests are plotted as a function of time in Figure 4. Similar results were observed in both systems in that peak eroding concentrations are reached relatively soon after the initiation of flow through the systems which then decay systematically until, at least in the case of the large fracture system, a possible steady-state erosion rate is observed.

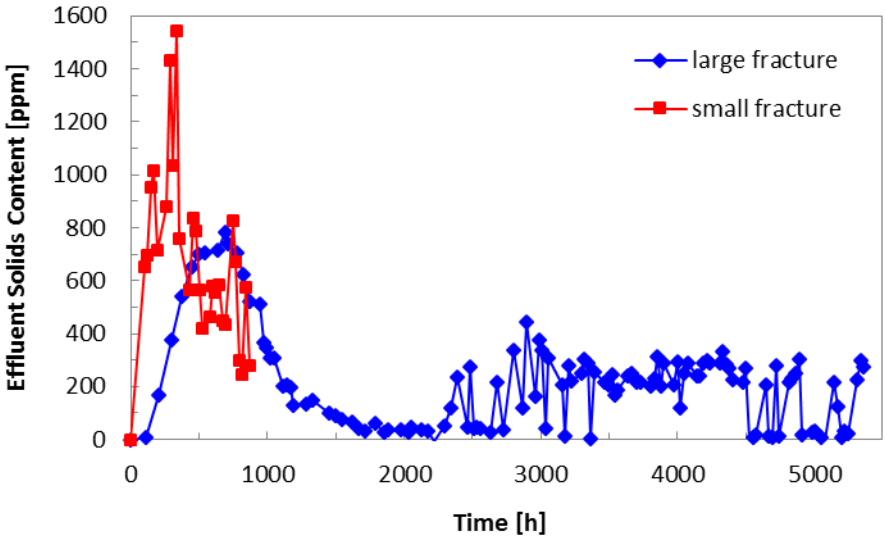

Figure 4. *Effluent solids concentrations observed over the course of the large and small fracture system tests with washed MX-80 bentonite against Grimsel groundwater simulant.*

Upon completion of the tests, the dry masses of the extruded and remaining (in the sample compartment) material fractions were determined. The results of these post-mortem analyses are specified in Table 1.

Table 1. *Sample mass analysis from the large and small fracture systems.*

Fracture System	**Emplaced Mass**	**Extruded Mass**	**Remaining Mass**	**Eroded Mass Fraction**
large	151.9589 g	24.9444 g	121.8176 g	3.3%
small	9.9934 g	1.7739 g	4.7606 g	33.3%

In principle mass loss results observed in the larger artificial fracture system can be compared to those from the smaller artificial fracture cell with the aim of deriving scaling arguments with respect to observed mass loss. However, the large and small fracture system tests reported here were not held constant with respect to aperture or flow velocity. Moreover, the larger artificial fracture system also has a larger initial sample volume which correspondingly requires a larger amount of sample mass than the smaller system at a given density (see Table 1). As such, any mass limiting effects encountered in the smaller cell may not be similarly reproduced in the larger system. It should also be noted that bulging deformations of the large system fracture plane were observed indicating that a constant 0.1 mm aperture condition was not preserved over the entire fracture plane area.

In order to try to assess the effect of scale through the experimental data, the observed mass loss results can be normalized to eroding surface area. Eroding surface areas of 3.14×10^{-4} m^2 and 1.04×10^{-4} m^2 can be calculated for the smaller and larger fracture systems, respectively, by taking into account the extrusion distances and idealized fracture apertures. Normalizing the average mass loss rates (kg/s), calculated from post-mortem mass determinations and test durations, observed for the small and large artificial fracture tests, one arrives at values of 111 $kg/m^2 \cdot yr$ for the small fracture system and 82 $kg/m^2 \cdot yr$ for the large fracture system. At face value it seems that the normalized rates are in reasonable enough accord to suggest that a similar linear scaling approach could be used to predict mass loss rates in horizontal fractures at repository scale provided extrusion distances are known or can be estimated.

The effect of flow velocity should be accounted for as well, as higher flow velocities should result in higher erosion rates. However, in both test systems substantial fracture volumes are occluded by sample extrusion. Additionally the fracture aperture in the large system is likely somewhat larger than 0.1 mm. These factors together imply that the flow velocities at the extruded interfaces in the two systems may not be as significantly different as they might first appear. Lastly the small fracture system does not appear to exhibit steady-state mass loss at the end of the test whereas the larger system possibly does (see Figure 4). This would result in an elevated mass loss rate for the small fracture system.

The comparison presented above is the result of only two tests. Before the normalized rates can be considered anything more than coincidental more tests should be performed.

Results from erosion experiments performed by ÚJV Řež, a. s.

The conceptual model was described in previous report, deliverable D2.2. The main aim of the erosion experiments is focused on the bentonite in saturation phase, where both the mechanical and chemical erosion is expected. The chemistry of flowing water have dominant impact on erosion process and its extent. Essentially, the stability of clay dispersion is given by the CCC of coagulant (e.g. cations or anionts in groundwater), which is a minimum concentration of coagulant that causes rapid coagulation. Knowing CCCs enable to decide about stability of clay dispersions in a given groundwater or experimental water based solution.

The czech concept of deep geological repository (DGR) considers the granite as a host rock and the hydrochemistry of groundwater from this granitic environment was summarised in previous report (Rukavičková et al., 2009). Three types of groundwater were identified in granitic Bohemian Massif: groundwater – meteoric water in contact with granite (depths 30 – 100 m), mineral groundwater – meteoric water in contact with granite and deep CO_2 and fossil groundwater – old saline waters. The expected chemistry of groundwater in DGR is a combination of these three types. However more groundwater analyses is needed from deeper horizons (300 – 1000 m) to verify the hydrochemistry. The following diagrams shows the main composition of these groundwater (Figure 1).

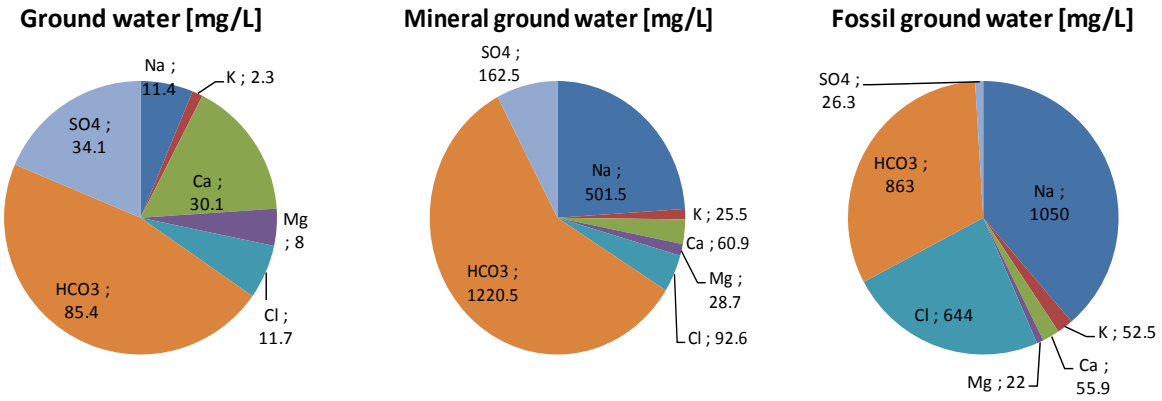

Figure 1.: Main chemistry of three groundwater types from granitic Bohemian Massif (after Rukavičková et al., 2009).

The coagulation experiments, where we study the coagulation of clay dispersions by inorganic cations and anions, suggested, that only for first type of groundwater (meteoric water in contact with granite) the bentonite dispersion should be stable. For other two types of groundwater the bentonite dispersions should coagulated. Because we expected a mixture of these three types of groundwater in the potential granite host rock, the groundwater chemistry is not favourable for long-term stability of bentonite colloids.

Experimental set-up and measurement

The experimental set-up differs from the set-up used by other groups in this project (see Figure 2) and it was described in deliverable D2.2. The main reason for this set-up was to use simple cylindrical arrangement with artificial granite fracture surrounded by compacted bentonite. The flow direction (from bottom to top) was selected mainly for avoiding of air bubbles capture within the apparatus and for homogenous saturation.

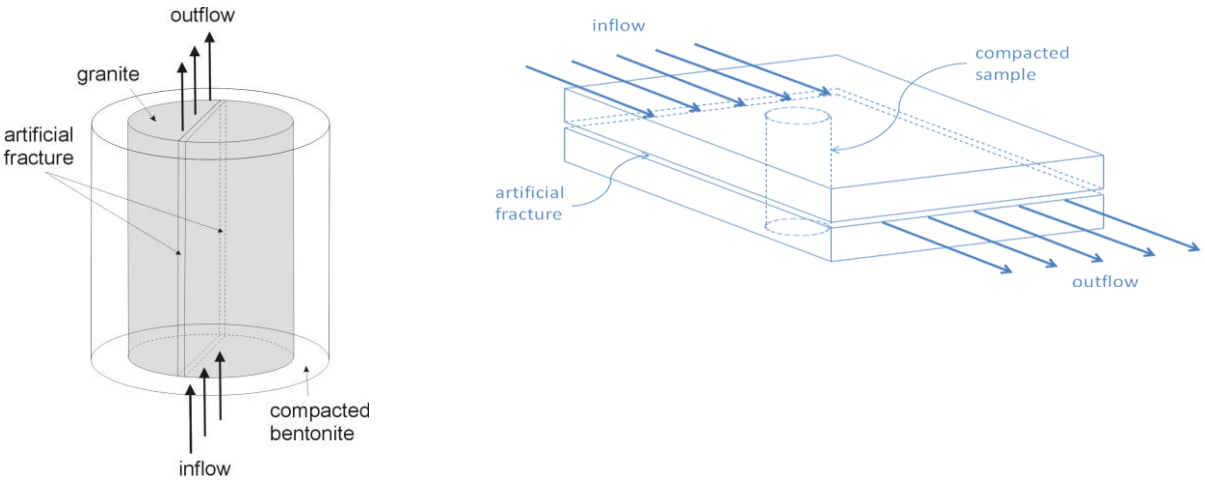

Figure 2.: Experimental set-up with artificial fracture in granite cylinder surrounded by compacted bentonite (ÚJV) – left. Experimental set-up with artificial fracture in between two acrylic blocks and compacted bentonite in the middle – right (Schatz et al., 2013).

Two methods were used for bentonite colloid concentration measurement. First one used Al concentration measured by inductively coupled plasma mass spectrometer (ICP-MS) as a indirect method for clay colloids concentration determination. Because the montmorillonite forms majority in bentonite (60 wt. % for bentonite B75) and therefore the Al content is dominant in comparison with other Al bearing minerals in bentonite, the Al can be used as a indirect tracer for clay colloids. The second method was based on a measurement with photon cross-correlation spectroscopy (PCCS). The calibration curve for estimation of bentonite colloid concentration can be obtained from plotting the response of the photomultiplier (kcps) vs. the known concentration of bentonite colloids (see Figure 3, left). The detection limit for this measurement with PCCS is around 1 mg/L. Comparison of results from both methods showed linear trend, but mainly for higher concentrations (see Figure 3, right). The scatter in low concentrations can be attributed to PCCS detection limit.

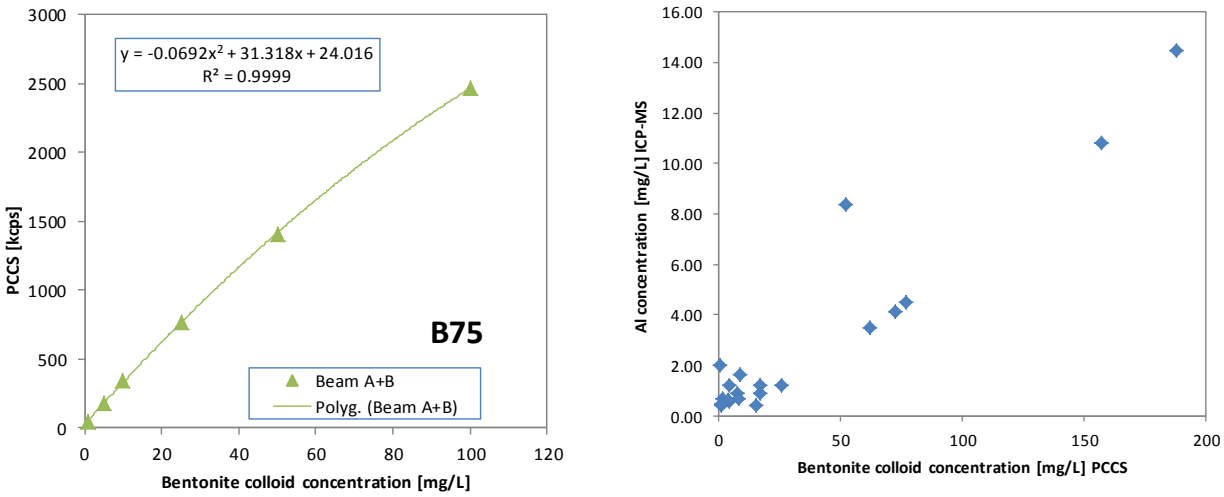

Figure 3.: Calibration curve for measurement of bentonite colloids concentration on PCCS – left. Comparison of both method for measurement of bentonite colloids concentration – right.

Results

The experimental results showed that the erosion rate at a given experimental arrangement reached from 0.4 to 55 kg/m^2/year at flow rates in the range of 5.37×10^{-6} – 2.48×10^{-4} m/s and fracture aperture in the range from 0.15 to 2 mm (Figure 4). The erosion experiments did not show a clear trend between the erosion rate and width of aperture, which is probably caused by the small set of experiments.

All experiments were carried out with distilled water which simulated groundwater with low ionic strength and therefore the extreme conditions with the highest rate of erosion. Mineral separation was observed (probably quartz and biotite) in experiments performed with small fracture aperture from 0.1 to 0.2 mm. This phenomenon may be particularly important mainly for the filtering effect, where the accumulations of small mineral grains can clog pores or fissures and thus prevent the bentonite erosion.

Generally, the chemical-mechanical erosion for Ca-bentonites is less significant than for Na-bentonites. However, it is necessary to consider the ion exchange between groundwater and bentonite, which can result in complete exchange of cations, and thus the selection of Ca- or Na-bentonite may not be the crucial issue.

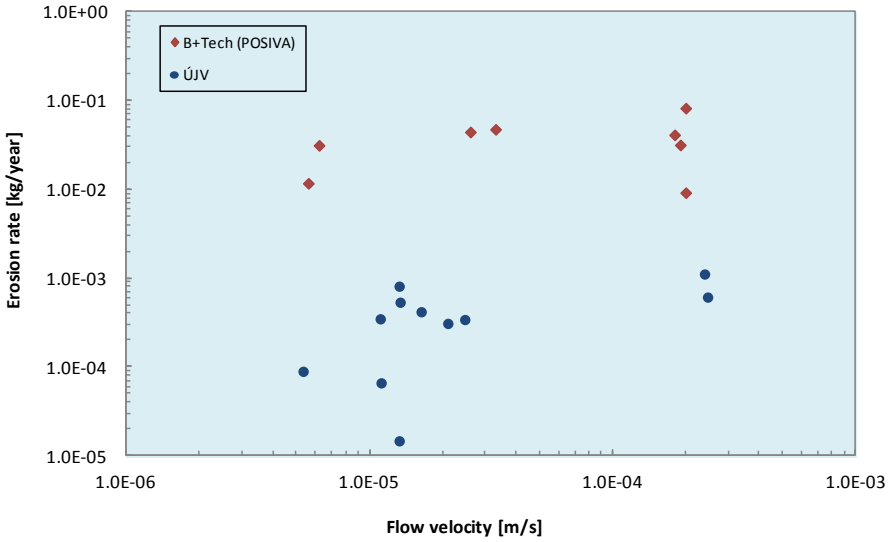

Figure 4.: Comparison of results: Erosion rate vs. flow velocity in log-log scale, blue points ÚJV results, red points POSIVA 2012-44 (Schatz et al., 2013). It has to be noted, that both sets of experiments are mainly differ in the fracture aperture (ÚJV fracture varies from 1.5×10^{-4} to 2.0×10^{-3} and B+Tech used just one size of fracture 1.0×10^{-3}) and liquid phase (ÚJV used only deionized water and B+Tech also NaCl electrolyte in some experiments). Also significant is the flow direction (see Figure 2).

References

Rukavičková L., Pačes T., Holeček J. (2009): Expertní odhad hydraulických a hydrochemických parametrů, DZZ 3.3 projektu „Výzkum procesů pole vzdálených interakcí HÚ vyhořelého jaderného paliva a vysoce aktivních odpadů“. ČGS Praha, 77 str.

Schatz T, Kanerva N, Martikainen J, Sane P, Olin M, Seppälä A, Koskinen K, 2013. Buffer erosion in dilute groundwater. POSIVA 2012-44. Posiva Oy, Olkiluoto, Finland.